# Resistance functions for spherical particles, droplets and bubbles in cylindrical tubes

By J. J. L. HIGDON and G. P. MULDOWNEY†

Department of Chemical Engineering, University of Illinois, Urbana, IL 61801, USA

Numerical computations are performed to evaluate the resistance functions for low Reynolds number flow past spherical particles, droplets and bubbles in cylindrical domains. Spheres of arbitrary radius $a$ and radial position $b$ move with arbitrary velocity $U$ within a cylinder of radius $R$. The undisturbed fluid may be at rest, or subject to a pressure-driven flow with maximum velocity $U_0$. The spectral boundary element method is employed to compute the resistance force for torque-free bodies in three cases: rigid solids, fluid droplets with viscosity ratio $\lambda = 1$, and bubbles with viscosity ratio $\lambda = 0$. A lubrication theory is developed to predict the limiting resistance of bodies near contact with the cylinder walls. Compact algebraic expressions are developed which accurately represent the numerical data over the entire range of particle positions $0 < b/(R-a) < 1$ for all particle sizes in the range $0 < a/R < 0.9$. The resistance functions are consistent with known analytical results and are presented in a form suitable for further studies of particle migration in cylindrical vessels.

## 1. Introduction

Low Reynolds number flow past spherical particles in cylindrical vessels is encountered in many areas of engineering application. Common examples include falling ball rheometers, hydrodynamic chromatography, membrane transport and particle transport in pipes. In other applications associated with liquid droplets or gas bubbles in capillary tubes, the sphere/cylinder geometry represents the appropriate model in the limit of strong surface tension. Owing to the technical importance of these applications, the motion of spherical particles in tubes has received much attention in the fluid dynamics literature. Early work in this area has been summarized by Happel & Brenner (1965), while a more recent survey is given by Hirschfeld, Brenner & Falade (1984). In the light of these works and additional reviews cited by Hirschfeld *et al.*, we shall not attempt a comprehensive literature survey, but limit our review to those contributions which set the context for the present effort.

We consider a spherical particle of radius $a$ whose centre lies a distance $b$ from the axis of a cylinder of radius $R$. In general, we suppose that the particle may move with velocity $U$ in an arbitrary direction, while the undisturbed fluid may be subject to a pressure-driven flow with parabolic profile and maximum velocity $U_0$. Previous studies of this problem have addressed a number of special cases involving asymptotic limits with respect to particle size or position. Early work reviewed by Happel & Brenner employed the method of reflections, harmonic expansions and similar techniques to

† Present address: Mobil Research and Development Co, Billingsport Rd, Paulsboro, NJ 08066, USA.

calculate the resistance of small particles where $a/R \ll 1$. These calculations include results for arbitrary position $b/R$ as long as the particle remains far from the wall, $R - b \gg a$. Complementary results for liquid droplets and bubbles with small $a/R$ have been given by Hetsroni, Haber & Wacholder (1970). For axisymmetric geometries, Happel & Brenner cite results for large particles with radii up to $a/R = 0.8$. Later authors (Coutanceau & Thizon 1981) have noted some inaccuracy in these results for the largest particle sizes and have provided more accurate results in such cases.

In the studies cited above, the analysis was limited to particle motion parallel to the cylinder axis. The general problem of a small particle moving with arbitrary velocity at an arbitrary position was addressed by Hasimoto (1976) and Liron & Shahar (1978). These analyses, for a Stokeslet singularity in a cylindrical tube, provide a solution for small particles to $O(a/R)$. While Hasimoto and Liron & Shahar presented their results in graphical form, Hirschfeld *et al.* (1984) revisited this problem and gave an extensive numerical tabulation of results for arbitrary positions. Falade & Brenner (1985) developed simple analytical expressions for these results in the asymptotic regime for particles close to the boundary but outside the lubrication regime, i.e. $a/R \ll 1$, $a \ll R - b \ll R$. The mathematical analysis for translating particles may be extended to the complementary problem of a rotating sphere in a cylindrical domain. Comprehensive results for this problem including a detailed comparison with previous work are given by Zheng, Powell & Strove (1992).

The small particle restriction for non-axisymmetric configurations has been addressed by a number of authors in recent years. Tozeren (1982, 1983) presented a solution for finite size particles as a perturbation expansion, valid for particles near the cylinder axis, $b/R \ll 1$. At the other extreme, Cox (1974) developed a general lubrication theory for solid surfaces near contact and included specific results for sphere/cylinder geometries. The analyses of both Tozeren and Cox break down in the limit as the particle radius approaches the cylinder radius, $a/R \to 1$. This limit, for a tightly fitting particle, has been studied by Bungay & Brenner (1973).

Despite the volume of research devoted to particle and droplet motion in cylindrical domains, there has been no complete solution valid for finite size particles moving with arbitrary velocity at arbitrary positions in the cylinder. In the present effort, we seek to address this deficiency through a comprehensive program of numerical computations. We include results for particle sizes up to $a/R = 0.9$ which are valid for all positions from the cylinder axis to the near contact lubrication regime. We consider translational velocities along each of the three coordinate axes as well as the effects of a mean pressure-driven flow. Results are presented for solid particles and for fluid droplets with relative viscosities of 0 and 1.

In the compilation of our results, the resistance force for each particle is given as an algebraic expression whose functional form is determined from known analytical results. The numerical coefficients are obtained from the detailed computational results together with known asymptotic limits. In this effort, we have followed the spirit of Jeffrey & Onishi (1984) who developed similar expressions for the resistance and mobility functions for the exterior problem of two spheres. By presenting our results in this form, we hope to facilitate the use of these results in future computations for engineering applications.

## 2. Formulation

We consider a spherical body of radius $a$ whose centre lies a distance $b$ from the axis of a circular cylinder of radius $R$. We choose a coordinate system with the $z$-axis along
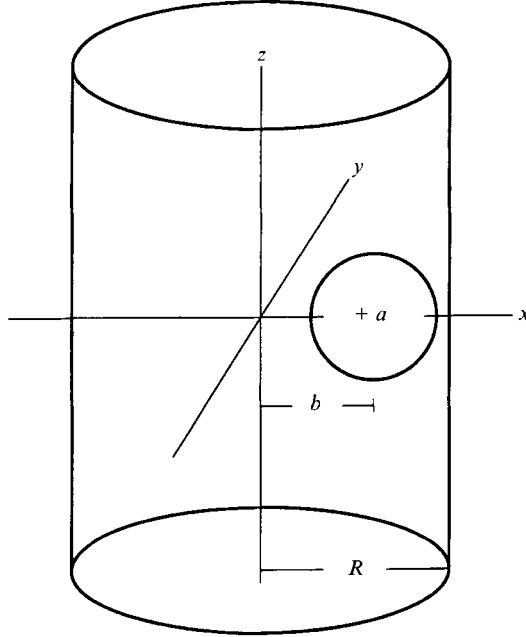
FIGURE 1. Coordinate system and geometry for a spherical particle in a cylindrical domain.

the axis of the cylinder, and choose the $x$-axis such that sphere is centred on the point $x_s = (b, 0, 0)$ (figure 1).

The governing equations are the Stokes equations for low Reynolds number flow together with the continuity equation,

$$-\nabla p + \mu \nabla^2 u = 0, \tag{1}$$

$$\nabla \cdot u = 0. \tag{2}$$

The boundary condition far from the sphere is given by

$$u = u^\infty \quad \text{as} \quad x \to \infty, \tag{3}$$

where the undisturbed velocity is a parabolic pressure-driven flow

$$u^\infty = U_0 \left( 1 - \frac{r^2}{R^2} \right) i_z \tag{4}$$

and $r^2 = x^2 + y^2$.

The no-slip boundary condition on the cylinder walls yields

$$u = 0 \quad \text{on} \quad r = R. \tag{5}$$

For a solid particle, we assume that the sphere translates with velocity $U$ and rotates with angular velocity $\Omega$. The no-slip boundary conditions on the sphere are then

$$u = U + \Omega \times (x - x_s) \quad \text{on} \quad |x - x_s| = a. \tag{6}$$

For a fluid droplet, we assume that the droplet has viscosity $\lambda \mu$ and surface tension $\gamma$. We consider the asymptotic limit as the capillary number $Ca = \mu U / \gamma \to 0$ and assume that the droplet maintains a spherical shape. The boundary conditions on the

sphere are the no-penetration condition for the normal velocity together with the continuity of shear stress across the interface. For a droplet translating with velocity $U$, this yields

$$\boldsymbol{u}\cdot\boldsymbol{n} = \boldsymbol{U}\cdot\boldsymbol{n}, \quad (\boldsymbol{f}_1-\boldsymbol{f}_2)\cdot(\boldsymbol{I}-\boldsymbol{n}\boldsymbol{n}) = 0 \quad \text{on} \quad |\boldsymbol{x}-\boldsymbol{x}_s| = a. \tag{7}$$

Here $\boldsymbol{f}=\boldsymbol{\sigma}\cdot\boldsymbol{n}$ and subscripts 1 and 2 refer to the interior and exterior of the drop respectively; $\boldsymbol{n}$ is the unit normal vector pointing out of the sphere.

The force and torque on the sphere are given by

$$\boldsymbol{F} = \int_{S_s} \boldsymbol{f}\mathrm{d}S, \qquad \boldsymbol{T} = \int_{S_s} (\boldsymbol{x}-\boldsymbol{x}_s)\times\boldsymbol{f}\mathrm{d}S, \tag{8), (9}$$

where the integration extends over the surface of the sphere $S_S$.

For both solid and fluid spheres, we assume that the translation velocity $U$ is specified, and we require that the torque on the body is zero:

$$\boldsymbol{T} = 0. \tag{10}$$

With these boundary conditions, we have a well-posed boundary value problem for the Stokes equations in the sphere/cylinder domain. This problem may be solved to determine the force on the particle $F$ as a function of the prescribed velocities $U$ and $U_0$. Owing to the linearity of the Stokes equations and the symmetries in the geometry, the force may be expressed in terms of resistance coefficients $\boldsymbol{R}$ defined by

$$\begin{bmatrix} F_x \\ F_y \\ F_z \end{bmatrix} = C\mu a \begin{bmatrix} R_x & 0 & 0 \\ 0 & R_y & 0 \\ 0 & 0 & R_z \end{bmatrix} \begin{bmatrix} U_x \\ U_y \\ U_z \end{bmatrix} + C\mu a [R_p] \begin{bmatrix} 0 \\ 0 \\ U_0 \end{bmatrix}. \tag{11}$$

The numerical coefficient $C$ is chosen such that the resistance coefficients approach 1 as the particle size approaches 0. Thus $C = 6\pi$ for solid particles and $C = 4\pi(1+\frac{3}{2}\lambda)/(1+\lambda)$ for fluid droplets. The four resistance coefficients $R_x$, $R_y$, $R_z$, $R_p$ are dimensionless quantities which are functions of particle size $a/R$ and position $b/R$ and for liquid droplets of viscosity ratio $\lambda$.

The boundary value problems described above may be solved by the boundary integral method. The boundary integral method for Stokes flow is based on the integral formula

$$u_k(\boldsymbol{x}_0) = -\frac{1}{4\pi\mu} \int_{S_s+S_B} (S_{ik}f_i - \mu T_{ijk}u_i n_j)\,\mathrm{d}S, \tag{12}$$

where $\boldsymbol{S}$ and $\boldsymbol{T}$ are defined by

$$S_{ik}(\hat{\boldsymbol{x}}) = \frac{\delta_{ik}}{|\hat{\boldsymbol{x}}|} + \frac{\hat{x}_i\hat{x}_k}{|\hat{\boldsymbol{x}}|^3}, \tag{13}$$

$$T_{ijk}(\hat{\boldsymbol{x}}) = -6\frac{\hat{x}_i\hat{x}_j\hat{x}_k}{|\hat{\boldsymbol{x}}|^5}, \tag{14}$$

$\hat{\boldsymbol{x}} = \boldsymbol{x}-\boldsymbol{x}_0$ and the unit normal vector $\boldsymbol{n}$ points into the suspending fluid.

This integral formula expresses the velocity at a point $\boldsymbol{x}_0$ on the boundary of the fluid as an integral of the velocity and stress over the boundary. The surface of integration extends over the entire boundary of the fluid, which includes the sphere surface $S_S$ as well as the outer boundary $S_B$. Details concerning the derivation of this equation may be found in recent monographs by Pozrikidis (1992) and Kim & Karilla (1991).

For fluid droplets, one may write equations of the form (12) for the interior and

exterior of the droplet. Combining the two results with the continuity of velocity and shear stress across the interface leads to equations

$$u_k(\mathbf{x}_0) = -\frac{1}{4\pi\mu} \int_{S_s} (S_{ik} \Delta f_i - \mu(1-\lambda) T_{ijk} u_i n_j) \, \mathrm{d}S$$

$$-\frac{1}{4\pi\mu} \int_{S_B} (S_{ik} \Delta f_i - \mu T_{ijk} u_i n_j) \, \mathrm{d}S, \quad \mathbf{x}_0 \in S_B, \quad (15)$$

$$(1+\lambda) u_k(\mathbf{x}_0) = -\frac{1}{4\pi\mu} \int_{S_s} (S_{ik} \Delta f_i - \mu(1-\lambda) T_{ijk} u_i n_j) \, \mathrm{d}S$$

$$-\frac{1}{4\pi\mu} \int_{S_B} (S_{ik} \Delta f_i - \mu T_{ijk} u_i n_j) \, \mathrm{d}S, \quad \mathbf{x}_0 \in S_S \quad (16)$$

for points $\mathbf{x}_0$ on the outer boundary $S_B$ and on the sphere $S_S$ respectively.

These equations, (12) for a solid particle and (15), (16) for a fluid particle, represent the foundation of the boundary integral method for Stokes flow. When combined with the appropriate boundary conditions, they yield a Fredholm integral equation for the unknown velocities and stresses on the boundary surface. For a solid particle, the no-slip boundary conditions prescribe the velocity on the particle surface, and the unknowns are the surface stresses $f$. For the fluid particles, the boundary conditions prescribe the normal velocity and the shear stresses, while the unknowns are the jump in normal stress and the tangential components of velocity.

In the integral equations formulated above, the domain of integration on the surface $S_B$ extends over the range $-\infty < z < \infty$. This infinite domain proves inconvenient for numerical computations, and we truncate the domain at planes $z = \pm L$. The new boundary surface $S_B$ now includes the cylinder walls $\{r = R, -L < z < L\}$ as well as the ends $\{z = \pm L, 0 < r < R\}$. The no-slip boundary condition on the cylinder wall remains the same, (5); however, we require a boundary condition on the ends of the cylinder. The simplest choice would be to set $\mathbf{u} = \mathbf{u}^\infty$ on the ends which guarantees the correct behaviour in the limit as $L \to \infty$. The difficulty with the velocity boundary condition is that it requires a large value of $L$ before the limiting behaviour is reached.

In place of the velocity condition, we choose stress boundary conditions on the ends of the cylinder, in the form

$$f_x = f_x^\infty, \quad f_y = f_y^\infty, \quad f_z = \pm p_0 \quad \text{at} \quad z = \pm L. \quad (17)$$

Here $f_x^\infty$ and $f_y^\infty$ represent the shear stress associated with the parabolic velocity field $\mathbf{u}^\infty$, i.e. a shear stress which increases linearly with $r$. The constant $p_0$ in the normal stress $f_z$ is unknown *a priori*, but is determined from the constraint that the total volume flow rate match that of the undisturbed velocity field $\mathbf{u}^\infty$. With the stress boundary conditions, the solution assumes the correct limit as $L \to \infty$ and approaches this limit more rapidly than the solution with velocity boundary conditions.

The boundary conditions (17) complete the specification of the integral equations for the Stokes equations.

## 3. Numerical algorithms

In this paper, we solve the boundary integral equations via a high-order discretization using the *spectral boundary element method*. In this approach, the boundary geometry is divided into a moderate number of macroelements, and all variables including the

geometry $x$ and the physical variables $u, f$ are discretized as Lagrangian interpolants in terms of two parametric variables $\xi$ and $\eta$. The base points $(\xi_i, \eta_j)$ for the interpolations are chosen as the zero of Legendre polynomials leading to interpolants which are equivalent to products of orthogonal polynomials. Convergence of the numerical discretization is achieved by increasing the order of the polynomial for a fixed set of elements. A detailed description of this algorithm is given in the accompanying paper by Muldowney & Higdon (1995).

In the present implementation, we employed three discretizations involving a total of 18, 28 and 44 elements respectively. The smallest number of elements was employed for particles with $a/R$ up to 0.7 located at positions away from the walls of the tube. The 28-element discretizations were employed for the larger particles, while 44 elements were employed in extreme cases of near contact with gap/particle radius as small as 0.01. The maximum number of interpolating points in each variable ranged from ten points for the 18- and 28-element geometry to nine points for the 44-element case. Independent calculations were performed to compute each component of the resistance tensor $R$, except for $R_p$ which was determined at the same time as $R_z$. Each of these independent calculations yields a boundary value problem with two planes of symmetry, yielding a four-fold reduction in the number of unknowns. All components of $R$ could in fact be computed simultaneously, but the resultant loss of symmetry would require a significantly greater computational effort. The largest number of unknowns in any run was 2673 for a 44-element run with nine-point interpolants. The majority of runs employed far fewer unknowns. Computations were performed on IBM RS 6000/375 workstations and on an 8-processor Silicon Graphics Challenge. C.p.u. times on the IBM ranged from a few seconds to 5 min for the largest runs. Single-processor runs on the SGI required approximately twice as long, while multiprocessor run times decreased in a nearly linear fashion with number of processors.

The interpolation points on the surface of the sphere were assigned by defining quadrilateral elements on the faces of a cube and projecting points from the centre to the sphere surface. Points on the cylinder walls were assigned at intervals of $\theta$ and $z$, while points on the ends were assigned at intervals of $\theta$ and $r$. Figure 2(a) illustrates the layout of elements on the cylinder and cube for an 18-element discretization. Figure 2(b) illustrates the discretization for a sphere of radius $a/R = 0.8$ near contact with the wall. Within each element, lines of constant $\xi$ and $\eta$ are plotted at equal intervals for clarity. The actual nodal lines employ the non-uniform spacing associated with the zeros of Legendre polynomials. Note that the quadrilateral elements on the ends of the cylinder include degenerate cases in which the elements reduce to triangles at the centre of the cylinder. This mapping in no way limits the performance of the spectral element algorithm. Additional examples employing degenerate elements are presented in Muldowney & Higdon (1995).

We begin our discussion of the numerical results with sample computations demonstrating the convergence of the spectral boundary element algorithm. The first series of computations shown in table 1 illustrates the convergence for an axisymmetric flow past particles of radius $a/R = 0.1, 0.5, 0.9$. For the two smaller particles, the resistance functions $R_z$ have converged with a relative error of $5 \times 10^{-7}$ with the 18-element discretization. By contrast, the 18-element results for $a/R = 0.9$ yield an error which is still of order $1.3 \times 10^{-3}$ at order $N_B = 9$. For these larger particles, the entire perimeter of the sphere at the plane $z = 0$ is near contact with the wall. Referring to figure 2(a), we see that the 18-element discretization employs a single element on each of the curve faces which places the near contact perimeter of the sphere along the centre
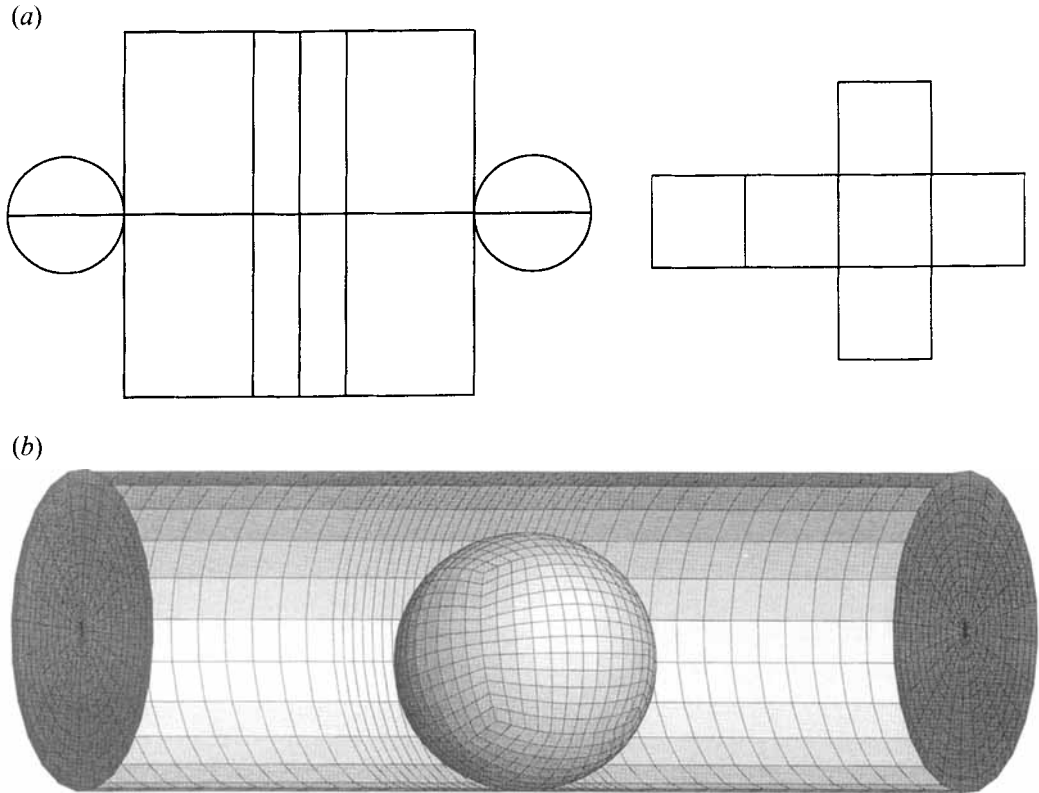
(a)



(b)



FIGURE 2. Discretization of geometry for spectral boundary element calculations. (a) Layout of element panels on cube and cylinder surfaces for 18-element discretization; points on the sphere are projected from the sphere centre to the surface of a cube. (b) Three-dimensional view of nodal lines for the panel layout of (a).

| $N_B$ | $a/R = 0.1$ | $a/R = 0.5$ | $a/R = 0.9$ | $a/R = 0.9$ |
|---|---|---|---|---|
| 4 | $-0.0027149$ | $-0.0589805$ | $287.6837$ | $-92.0239$ |
| 5 | $0.0000081$ | $-0.0025106$ | $-55.8795$ | $2.8510$ |
| 6 | $-0.0000058$ | $-0.0005531$ | $56.1884$ | $-0.6181$ |
| 7 | $-0.0000243$ | $-0.0000290$ | $-8.7406$ | $-0.0411$ |
| 8 | $-0.0000059$ | $-0.0000058$ | $5.6395$ | $0.0058$ |
| 9 | $-0.0000006$ | $0.0000009$ | $-1.5502$ | $-0.0005$ |
| 10 | $1.2632143$ | $5.9473753$ | $469.8196$ | $469.2225$ |

TABLE 1. Error is resistance coefficient $R_z$ for rigid spheres of radius $a$ centred in a cylinder of radius $R$. $N_B$ is the number of Lagrangian interpolation points in the spectral element discretization, and the last entry in each column is actual value of $R_z$. The first three data columns are for 18-element discretization; the final column for 28 elements.

of an element. The spacing of nodes based on Legendre polynomials gives high resolution near the edges of elements, but stretches points away from the centre of the elements. This feature combined with the element layout on the cube leads to poor convergence for large particles. To correct this deficiency, a 28-element discretization is used which employs additional elements on each cube face and places the contact perimeter at the edge of an element. With this modification, table 1 shows that the $a/R = 0.9$ computation converges to a relative accuracy of $1 \times 10^{-6}$.

| $N_B$ | $a/R = 0.1$ | $a/R = 0.5$ | $a/R = 0.9$ |
|---|---|---|---|
| 5 | 34.727 | 40.443 | 146.2 |
| 6 | 1.695 | 1.912 | 9.9 |
| 7 | 0.095 | −0.011 | 0.4 |
| 8 | 0.029 | 0.037 | 0.2 |
| 9 | 112.824 | 188.031 | 522.1 |

TABLE 2. Error in resistance coefficient $R_x$ for rigid spheres of radius $a$ in near contact with the wall of a cylinder of radius $R$. Gap size/particle radius = 0.01. The last entry in each column is actual value of $R_x$. All results are for 44-element discretization.

The next test case involves particles in near contact with the cylinder wall. Table 2 illustrates the convergence of $R_x$ for particles of radius $a/R = 0.1$, 0.5, 0.9 moving toward the wall. All calculations are for a gap equal to 0.01 of the particle radius with a 44-element discretization. This discretization includes additional smaller elements in the near contact region. In all cases, the resistance function $R_x$ has converged with a maximum relative error of $4 \times 10^{-4}$.

A variety of additional convergence tests have been conducted for other combinations of the system parameters. In all cases, the converged results show a relative error which is less than or equal to the error of $4 \times 10^{-4}$ found for the near contact region. In addition to these convergence studies, additional tests were conducted to test the sensitivity of the results to the parameter $L$ which is the half-length of the cylindrical domain. These tests show that a value of $L = 3R$ is sufficient to guarantee agreement with the asymptotic limit $L \to \infty$ with a maximum relative error of $2 \times 10^{-6}$ in the resistance functions $\boldsymbol{R}$. Given this accuracy, all results reported in this paper were computed with $L = 3R$. The fact that such a modest length is sufficient for asymptotic behaviour is associated with the rapid decay for Stokeslet singularities in a cylindrical domain (Liron & Shahar 1978).

## 4. Resistance functions for particles, droplets and bubbles

The principal goal of this paper is to provide convenient and accurate representations of the resistance functions for particles, droplets and bubbles at all positions within a cylindrical domain. Toward this end, we evaluated the resistance functions for each of the particle sizes noted below ranging from $a/R = 0.05$ to 0.9. Computations were performed for a number of particle positions ranging from the centre of the cylinder ($b/R = 0$) to near contact with a ratio of gap size/particle radius = 0.01. For each particle size, 14 values of $b/R$ were chosen to cover the range $0 < b/R < (1 - 1.2 \, a/R)$ where the upper limit guarantees a minimum gap/particle radius of 0.20. Ten additional values were chosen to cover the near contact region with gap/particle radius in the range 0.01 to 0.20. (The first group of computations were omitted for $a/R = 0.9$ since the entire range of $b/R$ lies within the near contact regime.) The results of these computations were employed to generate a least-squares approximation for each resistance function as described below. For brevity, we do not include the results of the individual computations in this paper; however, extensive tabulations of these results are available from the authors on request.

In selecting the algebraic form used to represent the resistance functions, we are guided by analytical results for three distinct regimes: (i) particles near the centre, $b/R \ll 1$, (ii) small particles in the vicinity of the wall $b/R \sim 1$, $a/(R - b) \ll 1$, and (iii) particles in the lubrication regime where the ratio of gap size to particle radius is small,

$(R-b-a)/a \ll 1$. In region (i), the method of reflections and asymptotic analysis (Happel & Brenner 1965; Tozeren 1982, 1983) show that the resistance functions are even functions of $b/R$. In region (ii), method of reflections calculations give resistance functions as power series in $a/(R-b)$. In region (iii), lubrication theory (described in the Appendix) yields the functional form and limiting behaviour of the resistance functions. Guided by these results, we proceed as follows.

First, we define a dimensionless position variable $\beta$

$$\beta = b/(R-a), \tag{18}$$

where $\beta = 0$ for a particle at the centre of the cylinder and $\beta = 1$ for a particle in contact with the cylinder wall.

Next, motivated by the behaviour in region (ii), we define a dimensionless variable $\rho$ to characterize the distance of a small particle from the cylinder wall. We might define $1/\rho$ as the ratio

$$\frac{a}{R-b} \equiv \frac{a}{R}\left[1 - \beta\left(1 - \frac{a}{R}\right)\right]^{-1}; \tag{19}$$

however, it proves to be more effective to define $1/\rho$ as an even function of $\beta$ to be consistent with the behaviour at small $\beta$.

Thus we define

$$\frac{1}{\rho} \equiv \frac{a}{R}\left[1 - \beta^2\left(1 - \frac{a}{R}\right)^2\right]^{-1}. \tag{20}$$

Finally, we define a dimensionless variable $\delta$ to characterize the gap size in the lubrication limit. One could employ the simple ratio of gap size to particle radius:

$$\frac{R-b-a}{a} \equiv \frac{R}{a}\left(1 - \frac{a}{R}\right)(1-\beta); \tag{21}$$

however, we again prefer to employ an even function of $\beta$, and thus define

$$\delta = \frac{1}{2}\frac{R}{a}\left(1 - \frac{a}{R}\right)(1-\beta^2). \tag{22}$$

Note that $\delta$ scales as the ratio of gap/particle radius in the limit as $\beta \to 1$, i.e. as the gap approaches zero. For convenience, define $\delta_0$ to be the value of $\delta$ evaluated at $\beta = 0$, which yields $\delta_0 \equiv (R-a)/2a$.

With these specifications, we define the following approximating functions:

$$\psi_0 = 1, \quad \psi_1 = \frac{a}{R}\beta^2, \quad \psi_2 = \frac{a}{R}\beta^4, \tag{23a-c}$$

$$\psi_3 = \beta^{2m}\frac{\beta^2}{\rho}, \quad \psi_4 = \beta^{2m}\left(\frac{\beta^2}{\rho}\right)^2, \tag{23d, e}$$

$$\psi_5 = \delta\left[\ln\left(\frac{\delta+1}{\delta}\right) - \ln\left(\frac{\delta_0+1}{\delta_0}\right)\right] - \beta^2\left(\frac{\delta_0}{\delta_0+1}\right), \tag{23f}$$

$$\psi_6 = \left[\ln\left(\frac{\delta+1}{\delta}\right) - \ln\left(\frac{\delta_0+1}{\delta_0}\right)\right] - \beta^2\left(\frac{1}{\delta_0+1}\right), \tag{23g}$$

$$\psi_7 = \frac{1}{\delta} - \frac{1+\beta^2}{\delta_0}. \tag{23h}$$

(a) $R_x$, $m = 2$

| $a/R$ | $c_0$ | $c_1$ | $c_2$ | $c_3$ | $c_4$ | $c_5$ | $c_6$ | $c_7$ |
|---|---|---|---|---|---|---|---|---|
| 0.05 | 1.098949 | 2.70920 | 0.28577 | 0.36899 | 0.43376 | 0.60510 | 0.23333 | 1.05228 |
| 0.10 | 1.218045 | 2.91771 | 0.43755 | 0.34092 | 0.48984 | 0.70359 | 0.21102 | 1.10957 |
| 0.20 | 1.537695 | 3.44426 | 0.85979 | 0.35226 | 0.98303 | 1.46740 | 0.16786 | 1.24226 |
| 0.30 | 2.019094 | 4.19574 | 0.92404 | 0.25470 | 1.01869 | 2.02905 | 0.06594 | 1.40615 |
| 0.40 | 2.770807 | 5.32638 | 1.37599 | 0.31312 | 1.39488 | 4.13763 | -0.08013 | 1.61374 |
| 0.50 | 4.006180 | 7.13868 | 2.14653 | 0.45835 | 1.89761 | 9.07757 | -0.34852 | 1.88562 |
| 0.60 | 6.196331 | 10.27428 | 3.78689 | 0.72899 | 2.85455 | 23.20219 | -0.85610 | 2.25877 |
| 0.70 | 10.577046 | 16.43808 | 7.95800 | 1.81102 | 4.67110 | 77.26027 | -1.80075 | 2.80883 |
| 0.80 | 21.464922 | 31.58564 | 17.56234 | 4.72437 | 6.93796 | 299.78758 | -4.35348 | 3.72678 |
| 0.90 | 66.290267 | 93.80967 | 35.05381 | 10.58720 | 5.17656 | 1393.89281 | -19.48100 | 5.74960 |

(b) $R_y$, $m = 1$

| $a/R$ | $c_0$ | $c_1$ | $c_2$ | $c_3$ | $c_4$ | $c_5$ | $c_6$ | $c_7$ |
|---|---|---|---|---|---|---|---|---|
| 0.05 | 1.098949 | 0.86475 | — | 0.14276 | -0.20788 | 0.00723 | 0.56103 | — |
| 0.10 | 1.218045 | 0.95416 | — | 0.13747 | -0.17164 | 0.07982 | 0.63309 | — |
| 0.20 | 1.537695 | 1.10651 | — | 0.11078 | -0.09792 | 0.30075 | 0.82208 | — |
| 0.30 | 2.019094 | 1.28260 | — | 0.11666 | -0.03833 | 0.71558 | 1.10159 | — |
| 0.40 | 2.770807 | 1.54751 | — | 0.15375 | 0.06547 | 1.57491 | 1.53690 | — |
| 0.50 | 4.006180 | 1.98635 | — | 0.24226 | 0.18096 | 3.41297 | 2.26274 | — |
| 0.60 | 6.196330 | 2.79580 | — | 0.42807 | 0.31949 | 7.84814 | 3.59350 | — |
| 0.70 | 10.577046 | 4.50932 | — | 0.83352 | 0.54598 | 20.89075 | 6.40611 | — |
| 0.80 | 21.464922 | 9.03423 | — | 1.93203 | 0.92453 | 73.92857 | 13.97542 | — |
| 0.90 | 66.290263 | 28.81166 | — | 6.68950 | 1.90797 | 537.30950 | 48.65043 | — |

**(c) $R_z$, $m = 2$**

| $a/R$ | $c_0$ | $c_1$ | $c_2$ | $c_3$ | $c_4$ | $c_5$ | $c_6$ | $c_7$ |
|---|---|---|---|---|---|---|---|---|
| 0.05 | 1.117271 | −0.73027 | 0.61976 | 0.14069 | −0.25577 | −0.05635 | 0.51948 | — |
| 0.10 | 1.263214 | −0.88509 | 0.77149 | 0.08617 | −0.22276 | −0.05934 | 0.54056 | — |
| 0.20 | 1.679480 | −1.30422 | 1.03602 | −0.06911 | −0.10952 | −0.06961 | 0.58844 | — |
| 0.30 | 2.370096 | −2.09561 | 1.61261 | −0.37053 | 0.11516 | −0.10934 | 0.64607 | — |
| 0.40 | 3.591374 | −3.63400 | 2.86225 | −1.02198 | 0.47497 | −0.26903 | 0.71722 | — |
| 0.50 | 5.947375 | −6.84239 | 5.83431 | −2.75132 | 1.34087 | −0.72455 | 0.80812 | — |
| 0.60 | 11.091896 | −14.32557 | 13.86957 | −8.22332 | 4.11603 | −1.73070 | 0.93008 | — |
| 0.70 | 24.675976 | −35.00613 | 39.22254 | −27.69947 | 14.32534 | −0.34743 | 1.10651 | — |
| 0.80 | 74.669898 | −113.70329 | 150.59592 | −121.23424 | 65.22268 | 78.24620 | 1.39754 | — |
| 0.90 | 469.222507 | −732.58970 | 1252.70861 | −979.70688 | 645.77045 | 7400.80980 | 2.04018 | — |

**(d) $R_p$, $m = 2$**

| $a/R$ | $c_0$ | $c_1$ | $c_2$ | $c_3$ | $c_4$ | $c_5$ | $c_6$ | $c_7$ |
|---|---|---|---|---|---|---|---|---|
| 0.05 | 1.115409 | −2.91282 | 2.23970 | −0.08064 | 0.13495 | — | — | — |
| 0.10 | 1.254795 | −3.07872 | 2.40311 | −0.22735 | 0.30582 | — | — | — |
| 0.20 | 1.634787 | −3.55069 | 2.67484 | −0.58220 | 0.63431 | — | — | — |
| 0.30 | 2.228978 | −4.37378 | 3.27405 | −1.09868 | 1.02282 | — | — | — |
| 0.40 | 3.215738 | −5.82431 | 4.56920 | −2.01511 | 1.61164 | — | — | — |
| 0.50 | 4.995340 | −8.53211 | 7.30253 | −3.87563 | 2.65400 | — | — | — |
| 0.60 | 8.613008 | −14.19404 | 13.70181 | −8.49174 | 5.01887 | — | — | — |
| 0.70 | 17.474031 | −28.20971 | 30.78302 | −21.69727 | 11.30819 | — | — | — |
| 0.80 | 47.620198 | −76.27367 | 93.93854 | −74.08759 | 34.81009 | — | — | — |
| 0.90 | 266.432020 | −417.14394 | 557.34338 | −477.12013 | 208.22109 | — | — | — |

TABLE 3. Resistance functions $R$ for rigid spheres in cylindrical tubes. Coefficients $c_i$ are defined in equations (24), (25). The exponent $m$ is defined for functions $\psi_3$, $\psi_4$ in (23). Coefficient $c_0$ is the resistance function for a sphere at the centre of the tube.

We have chosen to represent the resistance functions as a single continuous function over the entire range $0 < \beta < 1$. This decision dictates the form of the approximating functions $\psi_i$. The first three terms $\psi_0$, $\psi_1$, $\psi_2$ are determined by the asymptotic behaviour at small $\beta$. The next two terms $\psi_3$, $\psi_4$ take the form of the method of reflections contributions in region (ii) with the additional factors of $\beta^2$ to preserve the approximation in the small-$\beta$ limit. The last three terms $\psi_5$, $\psi_6$, $\psi_7$ are determined by lubrication theory as described in the Appendix. As $\delta \to 0$, these terms scale as $\delta \ln \delta$, $\ln \delta$ and $1/\delta$ respectively. In these three cases, we have defined the function $\psi$ by taking the appropriate lubrication result and subtracting the limiting behaviour for small $\beta$. As before, this serves to preserve the character of the approximation at small $\beta$.

Each of three components $R_x$, $R_y$, $R_z$ may now be expressed in the form

$$R_{x,y,z} = \sum_{i=0}^{7} c_i \left(\frac{a}{R}\right) \psi_i \left(\beta, \frac{a}{R}\right), \tag{24}$$

while the resistance coefficient for a particle held fixed in a parabolic flow field is expressed

$$R_p = \sum_{i=0}^{7} c_i \left(\frac{a}{R}\right) \psi_i \left(\beta, \frac{a}{R}\right) - \beta^2 \left(1 - \frac{a}{R}\right)^2. \tag{25}$$

The last term in (25) is equal to $(b/R)^2$ and is associated with the velocity profile for parabolic flow.

The coefficients in (24) and (25) are chosen to satisfy known asymptotic limits and to minimize the errors in a least-squares approximation to the numerical data.

With the definitions above, the primary results of this paper are listed in tables 3, 4 and 5.† These tables give the coefficients $c_i$ and exponent $m$ (for functions $\psi_3$, $\psi_4$) required to fit the numerically computed values of the resistance functions $R$. With the tabulated values, each resistance function is approximated with a maximum relative error of $1 \times 10^{-3}$. The error for the resistance functions $R_p$ is measured relative to the value of $R_p$ at the centreline, since the function $R_p$ itself approaches zero for a small particle approaching the cylinder wall. As noted above, up to 24 data points were employed in developing the least-squares approximations at each radius $a/R$. These data were fit by an approximating function with significantly fewer degrees of freedom (from five to eight unknowns) guaranteeing a smooth representation of the data. Owing to the degree of overconstraint, the error at arbitrary $\beta$ points will be well approximated by the error at the prescribed data points, i.e. $\leqslant 1 \times 10^{-3}$. Note that fewer data points in $\beta$ were required for the largest particle radius $a/R = 0.9$. At this radius, the entire range $0 < \beta < 1$ falls within the small-gap regime, and the resulting resistance function is significantly smoother than those for small $a/R$ which cover multiple asymptotic regimes.

Certain coefficients in each table have physical significance in appropriate asymptotic limits, while others are merely empirical values employed to obtain an accurate fit for the numerical data. In each table, the coefficient $c_0$ represents the resistance for a particle at the centre of the cylinder. All values of $c_0$ are accurate to a maximum error of $1 \times 10^{-6}$. The last coefficient in each table for $R_x$, $R_y$, $R_z$ represents the lubrication limit for a particle in near contact with the wall. These are the coefficients $c_7$ for the $1/\delta$ asymptote for $R_x$ and $c_6$ for the $\ln \delta$ asymptote for $R_y$ and $R_z$. For solid particles and for bubbles with $\lambda = 0$, these coefficients are determined from the exact lubrication

† Tables 4 and 5 are omitted for brevity. Copies of these tables may be obtained by contacting the Editorial Office or the authors. Electronic versions of all tables may be obtained by contacting the author (j-higdon@uiuc.edu) through electronic mail.

results given in the Appendix. For droplets with $\lambda = 1$, the coefficients $c_6$ for $R_y$, $R_z$ are taken from the Appendix, while the coefficient $c_7$ for $R_x$ is determined numerically from the least-squares approximation. The predicted value $c_7$ for droplets has an uncertainty of approximately 1 %.

While the numerical convergence studies guarantee the precision of the computed results, it is worthwhile to compare with previous authors to eliminate the possibility of systematic or conceptual errors. Toward this goal, several cross-checks were made to confirm the reliability of our results. As a first test, the axisymmetric results (in the form of $c_0$) for $R_z$ and $R_p$ were compared with the results of Haberman (Happel & Brenner 1965, table 7–3.2, 7–3.3) for solid particles. Excellent agreement was found up to particle sizes $a/R = 0.50$. For larger particles, Coutanceau & Thizon (1981) have pointed out the inaccuracy in Haberman's results and given corrected values. Our results are in complete agreement with Coutanceau & Thizon (their table 3) for the resistance $R_z$ for solids, droplets and bubbles.

For off-axis particles, we have compared our results with the theories of Hasimoto (1976) and Hetsroni *et al.* (1970). These authors give analytical results for the resistance functions for small particles $a/R \ll 1$. To compare with these results, we fit power series to the numerical results at small values of $a$ and $b^2$ and extracted the limiting behaviour. Our results were compared with those of Hetsroni *et al.* (equation (36)) for $R_z$ and $R_p$ to order $(a/R)^2$, $(b/R)^2$. All coefficients agreed within 1 % for solids, droplets and bubbles. This agreement is quite satisfying given that the higher coefficients are effectively determined from a second derivative of the numerical data in two separate variables, $a$ and $b$. For velocities in the off-axial directions, our limiting results were compared with those of Hasimoto (1976 and Erratum), and excellent agreement was found (within 1 %) with his coefficients for $R_x$, $R_y$ and $R_z$ up to order $(a/R)$ and $(b/R)^2$. Note that these comparisons are based on the extrapolations of our numerical results for small $a$ and $b$. These extrapolated values are not identical to the coefficients in tables 3–5. Those values are determined from a least-squares approximation to minimize the error in $\boldsymbol{R}$ over the entire range of $\beta$, while the extrapolated coefficients are optimized for the limit $a, b \rightarrow 0$.

For lubrication results, we have two independent checks of the present results. First, in the Appendix, we repeat the analysis of Cox (1974) for solid particles near a solid interface and extend these results to the case of fluid droplets near a solid boundary. In each case where analytical results are known, an extrapolation of the numerical results to zero gap size agrees with the analytical result to within 1 %. Finally, for large particles $a/R \rightarrow 1$, we compare $R_z$ with the asymptotic theory of Bungay & Brenner (1973, equation 4.68). The asymptotic theory for $R_z$ and $R_p$ agrees with our results with an error of 0.3 % at $a/R = 0.9$ and 1.3 % at $a/R = 0.8$. Based on these comparisons and on the detailed tests which confirm the numerical convergence, we believe that our computations yield reliable results for the resistance functions for spherical bodies in cylindrical tubes.

The final subject of this investigation is the extension of our tabulated results to particles of different radii. One approach would be to introduce more general approximation functions with two independent variables $a/R$ and $\beta$. All data for both variables could then be employed in a global least-squares approximation. Several attempts were made to develop approximation formula following this approach; however, these efforts were thwarted by the singular behaviour in the limiting cases, $(a/R \rightarrow 0)$, $(a/R \rightarrow 1)$, $(\beta \rightarrow 1$ as $\delta \rightarrow 0)$, $(\beta \rightarrow 1$ as $\delta \rightarrow \infty)$. A successful two-dimensional least-squares approximation would require the division of the parameter space into several distinct subregions with different approximations in each region. Similarly, we

considered applying a least-squares polynomial approximation in $a/R$ to the coefficients $c_i(a/R)$; however, this approach also requires domain subdivision for adequate performance. As an alternative to these procedures, we developed the interpolation approach described below.

The first step in interpolating the tabulated results to other radii $a/R$ is the choice of an appropriate independent variable. We note that the resistance coefficients as functions of $a/R$ possess a singularity as $a/R \to 1$, where the radius of the particle equals the radius of the tube. To improve the performance of the interpolation algorithms for $a/R < 1$, we map the singularity to infinity by defining a new variable $\alpha$:

$$\alpha = a/(R-a) \tag{26}$$

All interpolations are now performed using $\alpha$ as the independent variable.

There are two obvious strategies for interpolating $\mathbf{R}$ to particles of different sizes. The first approach is to calculate the resistance function at tabulated values of $a/R$ while holding $\beta$ constant at the desired value. These values may then be interpolated to produce the final value for $\mathbf{R}$. The second approach is to interpolate the values of the individual coefficients $c_i$ and to use the new coefficients together with $\psi_i$ to calculate $\mathbf{R}$. The direct interpolation of resistance values has the advantage that these functions are well-defined physical quantities. The disadvantage is that the slope $(\partial R/\partial a)$ is unbounded in the limit as $a \to 0$, $\beta \to 1$. The interpolation of the coefficients $c_i$ has the advantage that the singular slope $(\partial R/\partial a)$ at small $a$ is captured by the analytical form of the approximation functions $\psi_i$. On the other hand, the values of the higher-order coefficients $c_3$ to $c_5$ are relatively sensitive to small errors in the computed data especially at larger values of the radius. Given these trade-offs, we have performed a number of test computations to determine the optimal interpolation algorithm. Based on these tests, we recommend the following procedure.

(i) For small particles with $a/R < 0.1$, interpolate the *coefficients* $c_i$ using a four-point Lagrangian interpolant in the variable $\alpha$ based on the tabulated results for $a/R = 0.05$ through 0.3. The resulting coefficients will yield resistance functions with a maximum relative error of 1 % over the entire range $0 < \beta < 1$.

(ii) For larger particles with $0.1 < a/R < 0.9$, either the *coefficients* or the *resistance values* may be interpolated using a four-point Lagrangian interpolation in $\alpha$ based on the four nearest tabulated values of $a/R$. The direct interpolation of resistance values will yield higher accuracy at the larger particle sizes, but each approach yields results with a maximum relative error of 1 % for all particle sizes at all positions $0 < \beta < 1$.

With these extensions, the results of this paper provide simple analytical expressions for the resistance functions of spherical bodies in cylindrical tubes for all positions and all particle sizes from $a/R = 0$ to 0.9.

## Appendix

In this Appendix, we present expressions for the asymptotic form of the resistance functions based on lubrication theory for two surfaces in near contact. The development follows that of Cox (1974) for solid particles with appropriate extensions

for free surface boundary conditions. Cox presents a formal development of the asymptotic analysis with careful attention to the ordering of the equations and the magnitude of the various terms. We assume that the reader is familiar with this analysis and give only a brief sketch of the leading-order results.

Consider two surfaces in near contact such that the minimum distance between the surfaces is $h_0$. One surface, designated the *wall*, is assumed to be rigid and motionless, while the other surface, designated the *particle* may be either fluid or solid. Assume that each surface has finite curvature at the point of minimum separation and that the curvature is much less than $1/h_0$. Define a local Cartesian coordinate system with the origin on the wall at the point of nearest approach and the $x$-axis normal to the surfaces pointing toward the particle. (This choice of coordinates has each axis parallel to its counterpart in figure 1 but with the opposite sense.)

Let the rigid boundary wall be represented locally by

$$x = \eta_W = A_W y^2 + B_W z^2 \qquad (A\ 1)$$

and the particle surface (whether fluid or solid) represented by

$$x = \eta_P = h_0 + A_P y^2 + B_P z^2. \qquad (A\ 2)$$

Define $h(y, z)$ as the gap between the walls

$$h(y, z) = \eta_P - \eta_W = h_0 + A y^2 + B z^2 \qquad (A\ 3)$$

and define a variable $\zeta = x - \eta_W$ such that the gap between the surfaces occupies the region $0 < \zeta < h$.

We assume that $h_0 A$, $h_0 B \ll 1$ and note that changes in $y$ and $z$ scale with $1/A$ and $1/B$ while changes in $x$ scale with $h_0$. Under these circumstances, the lubrication approximation for the Stokes equations leads to the simplified form

$$\frac{\partial p}{\partial x} = 0, \quad \frac{\partial p}{\partial y} = \mu \frac{\partial^2 v}{\partial x^2}, \quad \frac{\partial p}{\partial z} = \mu \frac{\partial^2 w}{\partial x^2}. \qquad (A\ 4)$$

We consider the four separate cases of squeezing flow and of shearing flow of rigid particles and shear free fluid particles respectively. Consider first a squeezing flow for a rigid particle. The no-slip boundary condition on the wall is $u = (0, 0, 0)$ at $\zeta = 0$, while the no-slip condition on the particle is $u = (-U, 0, 0)$ at $\zeta = h$.

Integrating the Stokes equations twice with respect to $x$ and employing the boundary conditions yields

$$v = \frac{1}{2\mu} \frac{\partial p}{\partial y} (\zeta^2 - \zeta h), \quad w = \frac{1}{2\mu} \frac{\partial p}{\partial z} (\zeta^2 - \zeta h). \qquad (A\ 5)$$

The continuity equation, div $u = 0$, may be integrated with respect to $x$ and expressions (A 5) substituted for velocity components $v$ and $w$. Integrating the result from $\zeta = 0$ to $h$ yields an equation for $p(y, z)$:

$$\nabla \cdot (h^3 \nabla p) = -12\mu U, \qquad (A\ 6)$$

where $\nabla$ is the two-dimensional gradient operator in the variables $y$ and $z$. This is Cox's equation (3.9).

The solution of (A 6) is of the form $p = k_1/h^2$. Substituting for $p$ and solving for the coefficient yields

$$p = \frac{3\mu U}{A + B} \frac{1}{h^2}. \qquad (A\ 7)$$

The net force on the particle surface due to the pressure is $F = \int_S -p\mathbf{n}\,\mathrm{d}S$ which to leading order gives

$$F_x = \int_{-\infty}^{\infty} \int_{-\infty}^{\infty} -p\,\mathrm{d}x\,\mathrm{d}y = \frac{3\pi\mu U}{A+B} \frac{1}{(AB)^{1/2}} \frac{1}{h_0}. \tag{A 8}$$

For a sphere of radius $a$ near the wall of a cylinder of radius $R$, we have

$$A = \frac{1}{2a} - \frac{1}{2R}, \quad B = \frac{1}{2a}. \tag{A 9}$$

With these substitutions, the dimensionless force may be written

$$R_x = \frac{F_x}{6\pi\mu a U} = 2\left(\frac{R}{2R-a}\right)\left(\frac{R}{R-a}\right)^{1/2}\frac{a}{h_0}. \tag{A 10}$$

This result (minus the factor $a/h_0$ which is absorbed into $\psi_7$) provides the values for the coefficients $c_7$ in table 3(a). It is equivalent to Cox, equation (7.12) coefficient $K_{33}$.

Next, we consider the squeezing flow of a fluid particle with zero viscosity. In place of the no-slip boundary condition, we have no-penetration and zero-shear boundary conditions on the bubble. Proceeding as before, we solve for the pressure, obtaining

$$p = \frac{3}{4} \frac{\mu U}{A+B} \frac{1}{h^2} \tag{A 11}$$

which is exactly $\frac{1}{4}$ of the result for rigid surfaces.

This result might have been inferred from symmetry arguments based on two rigid particles approaching with a gap twice that of the bubble approaching a rigid surface. Evaluating the integrals for the pressure force, we find the dimensionless force:

$$R_x = \frac{F_x}{4\pi\mu a U} = \frac{3}{4}\left(\frac{R}{2R-a}\right)\left(\frac{R}{R-a}\right)^{1/2}\frac{a}{h_0}. \tag{A 12}$$

Here we have non-dimensionalized with respect to $4\pi\mu a U$ which is the appropriate factor for a bubble with zero viscosity. This result provides the values for the coefficients $c_7$ in table 5(a).

It is important to note that the solution (A 12) applies for the problem for a fluid bubble approaching a *rigid* surface. The case of two fluid bodies approaching contact yields a dramatically different result, as shown by Davis, Schonberg & Rallison (1989) for the axisymmetric case involving two spherical droplets. The simple results (A 7) and (A 11) for rigid particles and shear-free particles cannot be easily extended to droplets with finite viscosity. In this latter case, one must employ numerical methods to solve an integral equation for the flow interior to the fluid droplet. A discussion of this procedure for the case of axisymmetric bodies is given by Davis *et al.* In the present circumstances, we simply employ the spectral boundary element algorithm to determine the resistance functions. The extrapolated results for a liquid droplet with viscosity ratio $\lambda = 1$ yield the values of $c_7$ in table 4(a).

We now turn our attention to the problem of shearing flows for rigid particles. We assume that the particle velocity at the centre of the sphere is $\mathbf{u} = (0, V, W)$ and the angular velocity is $\mathbf{\Omega} = (0, \Omega_2, \Omega_3)$. The particle velocity at the contact point $(h_0, 0, 0)$ is then $(0, \tilde{V}, \tilde{W}) = (0, V - \Omega_3 a, W + \Omega_2 a)$. The no-slip boundary condition on the stationary wall remains as before; however, to leading order, the no-slip condition on the particle now becomes $\mathbf{u} = (\Omega_2 z - \Omega_3 y, \tilde{V}, \tilde{W})$ at $\zeta = h$.

Proceeding as before, we obtain a lubrication equation for $p$ which yields solutions of the form

$$p = (k_2 y + k_3 z)/h^2. \tag{A 13}$$

The no-slip boundary conditions yield values for the coefficients $k_2$ and $k_3$ in terms of $V$, $W$, $\Omega_2$ and $\Omega_3$. Evaluating the force and torque on the particle, we employ the condition of zero torque to solve for $\Omega_2$ and $\Omega_3$. The final results for the force on a torque-free rigid particle are

$$R_y = \frac{F_y}{6\pi\mu a V} = 2\left(\frac{R}{4R-3a}\right)\left(\frac{R}{R-a}\right)^{3/2}\ln\left(\frac{a}{h_0}\right), \tag{A 14}$$

$$R_z = \frac{F_z}{6\pi\mu a W} = 2\left(\frac{R}{4R-a}\right)\left(\frac{R}{R-a}\right)^{1/2}\ln\left(\frac{a}{h_0}\right). \tag{A 15}$$

These equations provide the values for the coefficients $c_6$ in tables 3($b$) and 3($c$) respectively.

Next, we consider the shearing motion of a zero-viscosity bubble. The no-penetration and shear-free boundary conditions apply as for the squeezing motion with the velocity now given by $u = (0, V, W)$. The solution for $p$ is of the form (A 13) with different values for the coefficients $k_2$ and $k_3$. Evaluating the pressure integrals gives the final expressions for the force on the bubble. In dimensionless form, we have

$$R_y = \frac{F_y}{4\pi\mu a V} = \frac{3}{2}\left(\frac{R}{5R-3a}\right)\left(\frac{R}{R-a}\right)^{3/2}\ln\left(\frac{a}{h_0}\right), \tag{A 16}$$

$$R_z = \frac{F_z}{4\pi\mu a W} = \frac{3}{2}\left(\frac{R}{5R-2a}\right)\left(\frac{R}{R-a}\right)^{1/2}\ln\left(\frac{a}{h_0}\right). \tag{A 17}$$

These equations provide the values for the coefficients $c_6$ in tables 5($b$) and 5($c$) respectively.

The shearing motion of a viscous drop with $\lambda = 1$ is closely related to that of the zero-viscosity bubble. In the case of a droplet, the shear stress is not zero everywhere, but the average shear stress must be zero in the lubrication region to satisfy the condition of zero torque on the body. Under these conditions, the lubrication force on the droplet is extremely close to that of the zero-viscosity bubble. Extrapolations based on the numerical data indicate the coefficients of the $\ln(a/h_0)$ term agree to within approximately 1 %. Given this agreement, we employ the analytical results for the shear-free bubble in determining the asymptotic coefficients for the droplets with $\lambda = 1$.

With the appropriate non-dimensionalization, this gives

$$R_y = \frac{F_y}{5\pi\mu a V} = \frac{6}{5}\left(\frac{R}{5R-3a}\right)\left(\frac{R}{R-a}\right)^{3/2}\ln\left(\frac{a}{h_0}\right), \tag{A 18}$$

$$R_z = \frac{F_z}{5\pi\mu a W} = \frac{6}{5}\left(\frac{R}{5R-2a}\right)\left(\frac{R}{R-a}\right)^{1/2}\ln\left(\frac{a}{h_0}\right). \tag{A 19}$$

These equations provide the values for the coefficients $c_6$ in tables 4($b$) and 4($c$) respectively.

## REFERENCES

BUNGAY, P. M. & BRENNER, H. 1973 The motion of a closely fitting sphere in a fluid-filled tube. *Intl. J. Multiphase Flow* 1, 25–56.

COUTANCEAU, M. & THIZON, P. 1981 Wall effect on the bubble behaviour in highly viscous liquids. *J. Fluid Mech.* 107, 339–373.

COX, R. G. 1974 The motion of suspended particles almost in contact. *Intl J. Multiphase Flow* 1, 343–371.

DAVIS, R. H., SCHONBERG, J. A. & RALLISON, J. M. 1989 The lubrication force between two viscous drops. *Phys. Fluids* A 1, 77–81.

FALADE, A. & BRENNER, H. 1985 Stokes wall effects for particles moving near cylindrical boundaries. *J. Fluid Mech.* 154, 145–162.

HAPPEL, J. & BRENNER, H. 1965 *Low Reynolds Number Hydrodynamics*. Prentice-Hall.

HASIMOTO, H. 1976 Slow motion of a small sphere in a cylindrical domain. *J. Phys. Soc. Japan* 41, 2143–2144 (and erratum, *J. Phys. Soc. Japan* 42, 1047).

HETSRONI, G., HABER, S. & WACHOLDER, E. 1970 The flow fields in and around a droplet moving axially within a tube. *J. Fluid Mech.* 41, 689–705.

HIRSCHFELD, B. R., BRENNER, H. & FALADE, A. 1984 First and second order wall effects upon the slow viscous asymmetric motion of an arbitrarily shaped, positioned and oriented particle within a circular cylinder. *Physiochem. Hydrodyn.* 5, 99–133.

JEFFREY, D. J. & ONISHI, Y. 1984 Calculations of the resistance and mobility functions for two unequal rigid spheres in low Reynolds number flow. *J. Fluid Mech.* 139, 261–290.

KIM, S. & KARRILA, S. J. 1991 *Microhydrodynamics: Principles and Selected Applications*. Butterworth-Heinemann.

LIRON, N. & SHAHAR, R. 1978 Stokes flow due to a Stokeslet in a pipe. *J. Fluid Mech.* 86, 727–744.

MULDOWNEY, G. P. & HIGDON, J. J. L. 1995 A spectral boundary element approach to three-dimensional Stokes flow. *J. Fluid Mech.* 298, 167–192.

POZRIKIDIS, C. 1992 *Boundary Integral and Singularity Methods for Linearized Viscous Flow*. Cambridge University Press.

TOZEREN, H. 1982 Torque on eccentric spheres flowing in tubes. *J. Appl. Mech.* 49, 279–283.

TOZEREN, H. 1983 Drag on eccentrically positioned spheres translating and rotating in tubes. *J. Fluid Mech.* 129, 77–90.

ZHENG, G.-H., POWELL, R. L. & STROEVE, P. 1992 Torque and frictional force on a slowly rotating sphere arbitrarily positioned in a circular cylinder. *Ind. Engng Chem. Res.* 31, 1190–1194.